Kinetics of Graphene Growth on Liquid Copper by Chemical Vapor Deposition

Valentina Belova[1,,‡], Hao Gao[2,‡], Wissal Sghaier[3], Anastasios Manikas[4], Mehdi Saedi[5], Hendrik H. Heenen[2,*], Costas Galiotis[4], Gilles Renaud[3], Oleg V. Konovalov[1], Irene M. N. Groot[5], Karsten Reuter[2], Maciej Jankowski[1]*

1 – ESRF – The European Synchrotron, 71 Avenue des Martyrs, 38043 Grenoble, France
2 – Fritz-Haber-Institut der Max-Planck-Gesellschaft, Faradayweg 4–6, 14195 Berlin, Germany
3 – Univ. Grenoble Alpes and CEA, IRIG/ MEM/NRS, 38000 Grenoble, France
4 – FORTH/ICE-HT and Department of Chemical Engineering, University of Patras, 26504 Patras, Greece
5 – Leiden Institute of Chemistry, Leiden University, P.O. Box 9502, 2300 RA Leiden, The Netherlands

KEYWORDS: CVD graphene, liquid metal catalyst, two-dimensional materials, radiation optical microscopy, growth kinetics, DFT calculations, machine learning potentials, molecular simulations

ABSTRACT: We report a combined experimental and computational study of the kinetics of graphene growth during chemical vapor deposition on a liquid copper catalyst. The use of liquid metal catalysts offers bright perspectives for controllable large-scale, high-quality synthesis technologies of two-dimensional materials. We carried out a series of growth experiments varying CH_4-to-H_2 pressure ratios and deposition temperature. By monitoring the graphene flake morphology in real time during growth using *in situ* optical microscopy in radiation mode, we explored the morphology and kinetics of the growth within a wide range of experimental conditions. Following an analysis of the flakes' growth rates, we conclude that the growth mode was attachment-limited. The attachment and detachment activation energies of carbon species are derived as 1.9 ± 0.3 eV and 2.0 ± 0.1 eV, respectively. We also conducted free-energy calculations by a moment tensor potential trained to density functional theory data. Our simulations propose that carbon dimers are most likely the active carbon species during growth, with attachment and detachment barriers of 1.71 ± 0.15 eV and 2.09 ± 0.02 eV, respectively, being in good agreement with the experimental results.

INTRODUCTION

Due to its outstanding electronic, optical, mechanical, and chemical properties, graphene (Gr) has major potential for a new generation of products and devices in a wide range of applications.[1,2] Since its isolation in 2004,[3] the research and implementation of graphene and other two-dimensional (2D) materials boosted in the electronic, medicine, sensor, energy, and space industries.[4,5] Chemical vapor deposition (CVD) is the state-of-art graphene production method.[6–8] However, as the standard CVD approach to graphene growth is based on the use of a solid catalyst substrate, it suffers from limitations in large-scale fabrication of high-quality, continuous graphene films. These solid substrates are often polycrystalline, displaying many grain boundaries, and have large expansion coefficients, at variance with graphene. Since graphene tends to grow in epitaxy on its substrate, the solid substrate morphology induces many defects (e.g. grain boundaries and then wrinkles upon cooling to room temperature) in the grown graphene. Meanwhile, CVD on a liquid substrate has a high potential for the advanced development of fast-growing, large-scale, single-crystal graphene production with a reduced density of defects. As proven in recent studies, the use of liquid metal catalysts largely improves the graphene quality thanks to the atomically smooth and homogeneous substrate surface and the absence of crystalline ordering. The liquid substrate thereby prevents epitaxial influence on the graphene flakes, promotes a reduced and uniform nucleation density, fast mass-transfer and carbon adatom and dimer diffusion as well as graphene flakes self-assembly.[9–12] Due to the high complexity of the growth mechanism governed by kinetics and thermodynamics, optimization of the controlling factors and conditions can be still quite challenging, especially when the growth mechanism is not well known, as is the case for graphene on liquid substrates.

In the graphene CVD process, a substrate surface, usually a metal like Cu, Ni, Pt, Fe, Ir, etc., acts as a catalyst for the decomposition of hydrocarbon precursor gas.[13] Copper has proven to be the best support for graphene due to its low solubility of carbon atoms and its low diffusion barrier, which allows for obtaining relatively large-area single-layer graphene (tens of μm) by the self-terminating growth.[14–18] The elementary processes taking place during the CVD growth of graphene on either solid or liquid copper are schematically illustrated in Figure 1. The catalyst substrate facilitates the chemisorption and dehydrogenation of precursor molecules such as methane, ethylene, or other hydrocarbons, resulting in carbon species such as monomers, dimers, etc.[19] The low solubility of C in Cu causes the formation of 2D surface gas of diffusing C species rather than diffusion into the bulk. The nucleation occurs when the concentration of carbon species reaches a supersaturation level C_{nucl}. The nucleation can also be induced by the presence of impurity nanoparticles acting as seeds.[20] Additional C species then attach to the initial nuclei, forming flakes

that grow in size (growth stage). Since the growth is a non-equilibrium process it continues until the equilibrium concentration of carbon active species C_{eq} on the copper surface is reached and the competing processes, *i.e.* attachment and detachment, are balanced. Besides the surface (intralayer) diffusion, C species can also undergo interlayer diffusion when climbing up the graphene flake and thus overcoming a step-edge energy barrier known as the Ehrlich–Schwoebel barrier.[21] There is also a continuing desorption of the precursor atoms/molecules from the surface which rate becomes significant at high temperatures as the sublimation of the metal substrate starts playing a role.

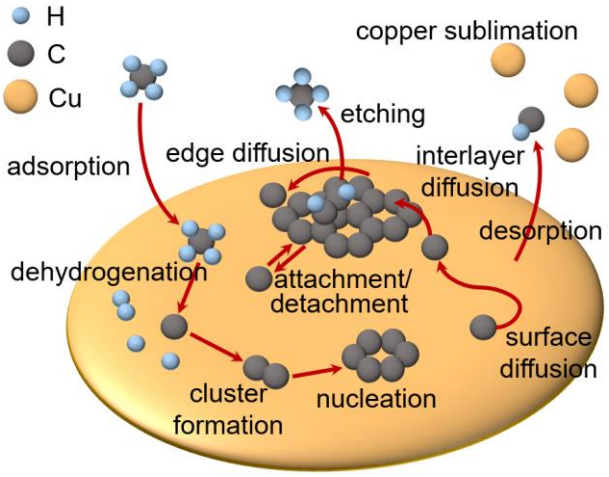

Figure 1. General illustration of the graphene CVD growth process on liquid Cu.

As just briefly discussed, CVD growth relies on a few elementary processes. While the parameters (e.g. pre-exponential factors and activation energies) are relatively well known for solid substrates,[22–25] very little is known for liquid substrates, and the values e.g. of surface diffusion of the different species, are expected to differ by orders of magnitude from those on solid surfaces. Until recently, the studies carried out on graphene grown on liquid copper were based on *ex situ* post-growth characterizations that entail a significant loss of information.[26,27] Thus, a detailed understanding of the mechanisms and kinetics of graphene domains grown on liquid copper, which is necessary for controlling the growth parameters and optimizing the synthesis of large-area single-crystal graphene domains, is still lacking.

Here, we use *in situ* methods in real time to study experimentally the kinetics of the graphene growth during CVD on liquid copper, and we combine these experiments with calculations.

Specifically, we use the multi-technique, multi-scale and real-time *in situ* characterization of high-quality single-layer graphene (SLG) growth by CVD on liquid metal catalyst (LMCat) recently proposed by Jankowski et al.[12] It was shown that the SLG flakes above 20 µm could be visualized and monitored as a function of time by radiation-mode optical microscopy due to the difference in emissivity between SLG and liquid copper at high temperatures (~ 1370 K).

One of the most common theoretical approaches for the description of thin-film growth is molecular simulation.[28] Here, we apply this method to investigate *in situ* the kinetics of the graphene growth and the morphology evolution during CVD on liquid copper. We propose a growth mechanism based on the investigated kinetics and support our findings using an enhanced sampling method. *Via* involved free-energy surface calculations using enhanced sampling based on a carefully trained machine-learning potential, we predict the activation energy for the proposed rate-determining step, and we find a quantitative matching our experimental observations.

RESULTS AND DISCUSSION

Procedure and quality control. As mentioned above, graphene was grown on a customized CVD reactor and the detailed experimental procedure is illustrated in Figure 2 and Movie 1. For graphene, C_{nucl} is known to be significantly higher than C_{eq}.[29] Therefore, we first applied a high CH_4 partial pressure (P_{CH4}/P_{H2} between $1.81-2.72\times10^{-2}$) to facilitate flake nucleation and accelerate the growth of the first flakes, then we monitor the flakes' evolution for a few minutes until their coalescence. Then we turned off the methane flow to initiate the etching of the flakes in the H_2/Ar atmosphere ($P_{CH4}/P_{H2} = 0$). As soon as only a few tiny islands were left on the surface, we changed the methane flow to an intermediate partial pressure value (*e.g.* $P_{CH4}/P_{H2} = 1.27\times10^{-2}$ in Figure 2), and the growth process was carefully followed and analyzed. Note, that in the regime of medium flows ($0.54 < P_{CH4}/P_{H2} < 1.81\times10^{-2}$) continuous nucleation still occurs, although its density and rate are reduced. In order to cover a broad growth rate range, the cycle of etching and regrowth at different P_{CH4}/P_{H2} was repeated several times for all five temperatures. For each image frame, the averaged flake area A, the diameter or the long diagonal (for the irregular shapes), the circumference L, and the circularity of the flakes were extracted.

Quality control of graphene samples that were grown on liquid Cu has been performed via Raman spectroscopy after a wet transfer on Si/SiO_2 wafers. The growth of monolayer graphene is confirmed by Raman spectra through the I_{2D}/I_G ratio. The corresponding analysis is provided in the Supporting Information (SI), Figures S1-S3.

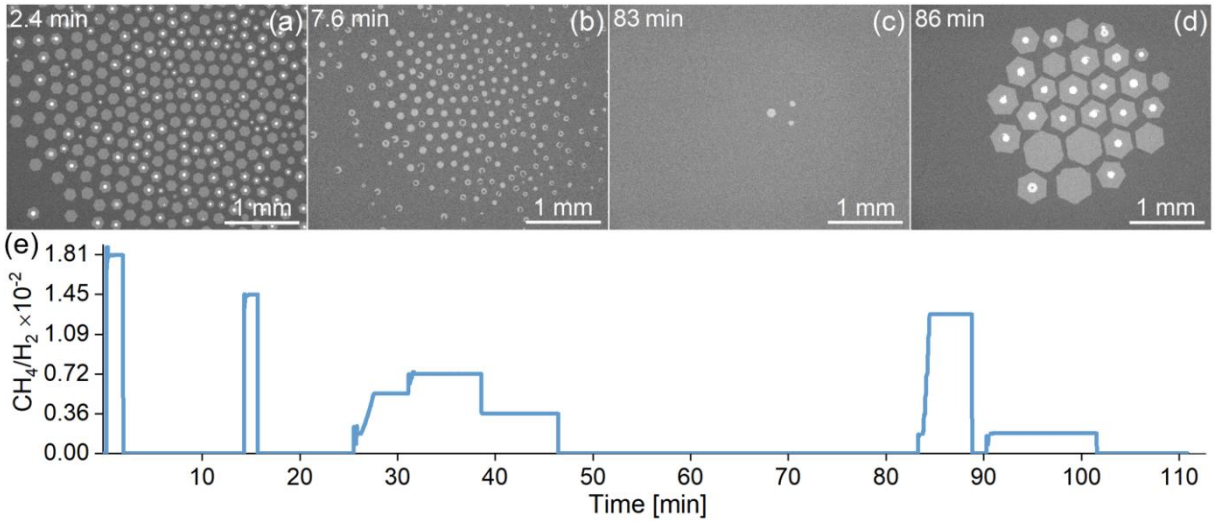

Figure 2. *Top:* Experimental steps of CVD graphene growth on liquid Cu at T = 1368−1456 K: (a) initial nucleation and growth of flakes at a high partial CH_4 pressure (P_{CH4}/P_{H2} between $1.81–2.72\times10^{-2}$); (b) etching ($P_{CH4}/P_{H2} = 0$); (c) and (d) regrowth with a lower flow of methane (here, $P_{CH4}/P_{H2} = 1.27\times10^{-2}$). The time is set to 0 s when the methane valve is opened for the first time. See also Movie 1. *Bottom:* (e) Time evolution of the gas pressure ratio corresponding to the images (a)-(d).

Flake morphology. First, we visually examined the variation of the growing flake morphology and found it to be dependent on growth time and pressure. The observed morphological behaviors can be roughly categorized into five modes depending on the ratio between methane and hydrogen pressures P_{CH4}/P_{H2} (Figure 3). The quantitative illustration of the shape evolution with the flake size for different pressure ranges can be found in the SI (Figures S4, S5). We note, that we do not see any prominent impact of the temperature on the morphology within the accessible range of T (~ 100 degrees) but rather on the growth and etching rates as will be shown in the following subsection.

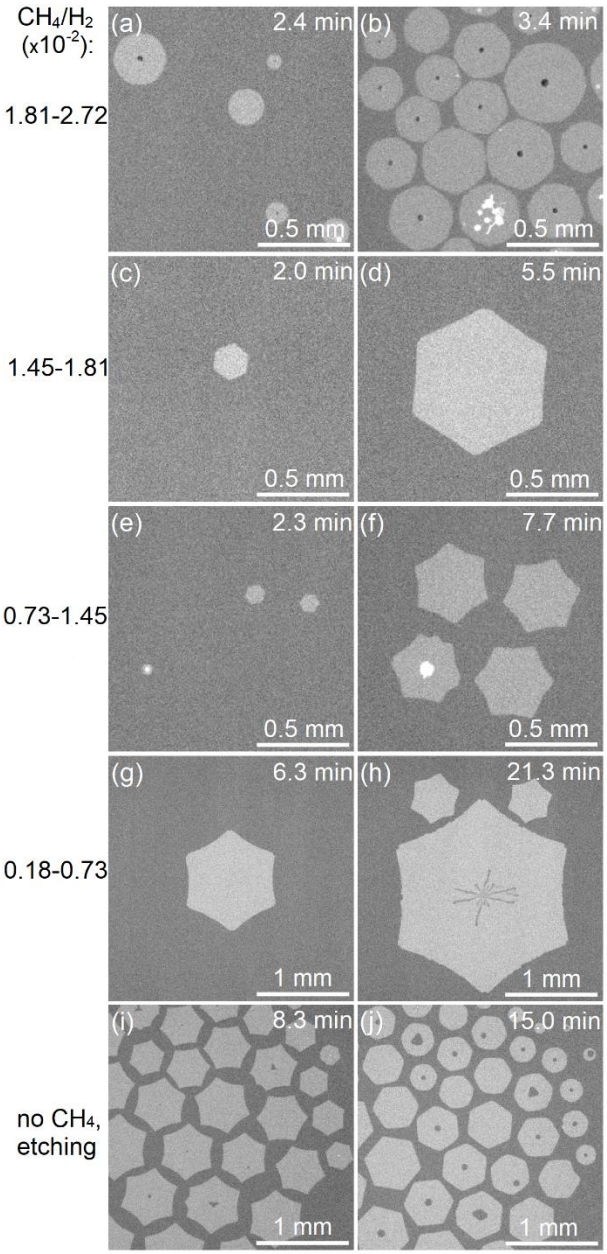

Figure 3. Radiation-mode optical microscopy images for different methane/hydrogen partial pressure ratios. The images in one row are not necessarily from the same growth experiment but present examples of the typical morphologies. Zero time is the moment when the methane flow is set to the indicated value. The green and red colors indicate the difference between the edges with a high and low accessibility for C adatoms.

For the highest CH_4 flows (P_{CH4}/P_{H2} = 1.81–2.72×10^{-2}, when the nucleation goes continuously, Figure 3a, b), the flakes have a well-defined circular shape that does not undergo noticeable changes during growth. When the content of CH_4 is lower but still relatively high (P_{CH4}/P_{H2} = 1.45–1.81×10^{-2}, Figure 3c, d), the flakes start to grow directly as perfect hexagons and at later stages develop a week tendency to concave edges. For medium CH_4 flow (P_{CH4}/P_{H2} = 0.73–1.45×10^{-2}, Figure 3e, f), the transition from the initial hexagonal to the concave dodecagon shape is faster and is more

pronounced with the external angle reaching 10° (Figure S4b). At low CH_4 flow (P_{CH4}/P_{H2} = 0.18–0.54×10^{-2}, Figure 3g, h), the flux of C adatoms is too low to initiate the nucleation, but if graphene flakes are already present on the surface they continue to grow forming sharp concave dodecagon with the external angle up to 20° (Figure S4a). In parallel, after reaching a certain size, the flakes start to etch at their center, where the availability of adatoms is minimal. Indeed, C mono- or di-mers that result from the dissociation of methane occurring at the Cu catalyst surface (not on graphene) have to overcome the Cu-C step-edge Ehrlich-Schwoebel potential barrier to reach the flake centers. Also, many flakes nucleate around a particle, *e.g.* an oxide particle, which would not be visible in the optical microscope. The presence of that particle playing the role of a defect may also cause enhanced etching at the center. When the methane flow is turned off (P_{CH4}/P_{H2} = 0, Figure 3i, j), the etching of graphene starts at the outer edges, and in the middle of the flakes if defects are present. In this pure etching regime, the edges closest to the vertices of concave dodecagons are etched faster. This leads first to the reverse transition when the hexagons with small protrusive corners and flattened edges in between are formed. The corners begin to smooth out at a later stage, and the flakes tend to transform into uniform circular disks.

The processes governing the flake shape could be related to the edge diffusion of atoms/species along the flake edge. In general, the edge-species diffuse from high-free-energy edge areas to low-free-energy ones. The thermodynamics equilibrium shape of graphene flake is hexagonal, in which everywhere on the edges has equal free energy as derived from Wulff construction.[30] In the beginning of the growth, the distribution of C species on the LMCat is homogeneous and hence isotropic at high methane pressure. Therefore initially, there is a tendency to an isotropic *i.e.* circular shape for an as-nucleated flake. However, circle is not the equilibrium shape of a graphene flake. Thus, the edge diffusion starts to play a role and drives the flake shape towards hexagon. When the hexagonal shape develops in time, that breaks the isotropy of radial diffusion, and hence the azimuthal uniformity of adatom concentration nearby the flake. The protruded hexagon corners start to attract more diffusion flux, making them to become even more protruded, leading to a dodecagon shape. The edge diffusion still tries to bring back the shape to perfect hexagon, but as flake size (and hence the edge length) grows, the edge diffusion becomes more and more limited. Consequently, the shape develops toward more pronounced concave dodecagon. We thus assume, that the observed flake shape development would not be due to increase of the C species diffusion limitation on the LMCat surface. Although at first, the circular symmetry of C species diffusion/distribution around the flake breaks to 6-fold symmetry, caused by flake edge diffusion driving the flake shape towards hexagon, leading to the observed circle to hexagon flake evolution. Next, edge diffusion becomes increasingly limited, caused by growing flake size, leading to the observed hexagonal to dodecahedron flake evolution.

Growth rates and experimental E_a. In this work, we defined the flake growth (or etching) rate as a change of flake lateral size over time. Since the shape of the graphene flakes observed is not constant, as a parameter of the lateral size we consider the effective radius R_{eff} described as the ratio between the flake area A and circumference L:

$$R_{eff} = \frac{2A}{L}. \quad (1)$$

The average R_{eff} (with a standard deviation of 20%) was found to increase (or decrease in the case of etching) linearly with time as demonstrated in Figure S6. Surprisingly, the linear trend is traceable over the broad pressure and temperature ranges, and, despite the shape transformations discussed above, no deviation from the linear law is observed. The negative slope of some curves in Figure S6 indicates etching at CH_4 flow below a certain threshold, i.e., at P_{CH4}/P_{H2} between 0.18-0.36×10^{-2}. Note that we consider here growth stages that are relatively far from the flakes' coalescence and closure of the layer so that the majority of the flakes have some degree of freedom as illustrated by exemplary Movie 1.

In previous studies, when CVD graphene growth on the solid copper catalyst was studied,[22,23,25] graphene growth rates were often defined as a change in area. However, we find here that the flake area grows proportionally to the square of time, which correlates directly with a linear evolution of the radius. As a consequence, the areal growth rates are not constant with time and depend linearly on the growth stage (flake size) as demonstrated in Figure S7. Using those in the Arrhenius equation may result in an inaccurate E_a value. Therefore, we choose here the R_{eff} as the main parameter of the growth description.

Recent theoretical studies by Seki et al.[31,32] predict two regimes of growth of isolated graphene domains (*i.e.* no interaction with other domains is considered). When the domain size is smaller than the diffusion length of the C adatoms on the surface, the growth rate of the domain is independent of the domain radius, and the growth is limited by the reaction in general. On the other hand, when the domain size is larger than the diffusion length, the growth is diffusion-limited and the domain area is proportional to time (the radius of the domain is proportional to the square root of time). The fact that the average R_{eff} grows with a constant rate independently of the flake size (in this study we observed flakes from 20 μm up to 2 mm in diameter), implies that carbon adatoms are always available at least around the flakes and the attachment process and the global concentration of C species primarily govern the growth. As we consider the growth of the flake equivalent radius of the circle corresponding to the area, in such a way, there is some cancelling between faster growing areas and slower growing areas in case of the non-compact shapes. Therefore, we conclude that we have attachment/detachment-limited growth. Following the observation that the lateral flake size is independent of time even for low CH_4 pressure (*e.g.* in

contrast to this work[23]), we can rule out the precursor dissociative adsorption as the rate-limiting step under our experimental conditions. We note, that a noticeable deviation of the lateral growth rates from the observed linear evolution of the radius as a function of time appears only at the latest growth stages when the flakes approach coalescence and closure of the layer (See Figure S8 and Movie 2).

The linear growth rates of graphene flakes on liquid copper are presented in Figure 4a as a function of P_{CH4}/P_{H2} and T. Up to a critical value of $P_{CH4}/P_{H2} = 1.63\times10^{-2}$, the growth rates are found to increase almost linearly with P_{CH4}/P_{H2} at all T. Then, above $P_{CH4}/P_{H2} = 1.63\times10^{-2}$, the evolution with pressure deviates from linear towards lower rate values. The $P_{CH4}/P_{H2} \approx 0.27\times10^{-2}$ at which the growth rate is around zero should correspond to the C_{eq} of carbon adatoms on the liquid copper surface since the attachment and detachment rates are balanced in this case. The increase of the CH_4 flow leads to an increase in the actual carbon concentration C. The growth rate's linearity at low CH_4 flow agrees with the classical film growth theory where the edge growth rate is proportional to a degree of supersaturation C - C_{eq}.[33] The deviation from linearity can be related to both, the saturation of the Cu surface with C species and the dual role of H_2 as discussed further.

The presence of hydrogen is vital in the CVD process.[25,27,34,35] On the one hand, it is assumed to participate in methane dehydrogenation, creating sites for hydrocarbon radicals and thus facilitating the formation of the active C species, although a precise understanding of the detailed mechanism is still missing. On the other hand, H_2 etches the graphene, predominantly attacking defects and terraces above the first layer if there are any. Thus, to secure the growth of high-quality graphene, the partial pressure P_{H2} can be used to control the size and morphology (compact circular or hexagonal vs dendritic/random shapes such as 'snowflakes' or 'flowers') of the islands and usually has to exceed many times the partial pressure of methane P_{CH4}.[27,34,36,37] If the concentration of the hydrocarbon precursor is too low, the etching process dominates, and the grown graphene flake is etched-out.

Although the growth at higher methane pressure cannot be followed with the same accuracy due to the high nucleation density and fast layer closure, we also explored the range of partial pressure of H_2 between 0 (no H_2 flow) and the default value of 18.18 mbar (as in the gas mixture of 200 sccm of Ar and 20 sccm of H_2) by using 5 % concentration of CH_4 in Ar with the highest flow of 45 sccm, the highest flow of H_2 was 20 sccm, and the total flow was in the range of 220-265 sccm (Figure 4b). The growth rates reach the maximum around $P_{H2} = 9.65$ mbar that corresponds to a CH_4/H_2 ratio of 0.19 and then declines with the decrease of P_{H2} down to zero. This bell-shaped dependence of the growth rates on the P_{H2} is in good agreement with previous studies on solid substrates and confirms that the presence of H_2 is crucial in the CVD process.[25]

The CVD process is thermally activated and its general rate is limited by the slowest reaction step; *i.e.* the one having the highest energy barrier. However, as it is a complex reaction with many intermediate steps, an apparent activation energy E_a might be time-dependent following the process stages. Nevertheless, for primary reactions, their E_a can be derived from the temperature dependence of the reaction rate by using the Arrhenius equation. The corresponding Arrhenius plots of the growth rates are shown in Figure 4c. As expected, the growth rate increases with the substrate temperature. However, as can be seen, the dependence is non-linear in the Arrhenius coordinates. Thus, for the lowest data sets (P_{CH4}/P_{H2} = 0.18×10^{-2} and 0.36×10^{-2}) etching starts to dominate over growth with increasing T leading to a decrease of the growth rate. These two opposite processes, growth and etching, are at play simultaneously and at low methane content, we assume that the detachment of C atoms is mainly due to the etching by hydrogen. To fit the data correctly, the Arrhenius law has to include both activation energies: attachment and detachment:[38]

$$GR = aP_{CH4}e^{-\frac{E_{att}}{kT}} - bP_{H2}e^{-\frac{E_{det}}{kT}}, \quad (2)$$

where GR stands for 'growth rate', a and b are constants, and k = 8.63 × 10^{-5} eV K^{-1} atom^{-1} is the Boltzmann constant.

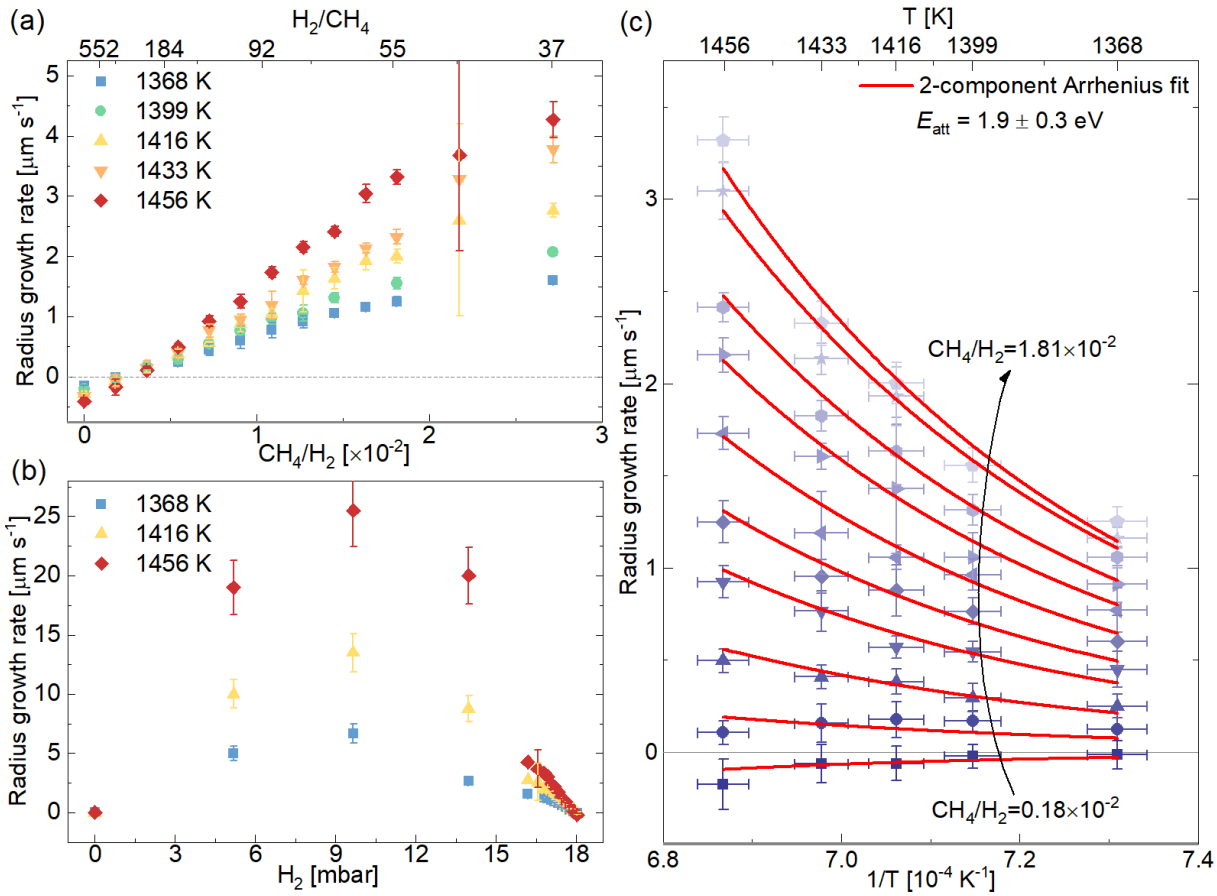

Figure 4. Graphene flakes' growth rates on liquid Cu at a total pressure of 200 mbar and total gas flow of 220−265 sccm: (a) lateral growth rates plotted as a function of partial pressures and T for

low ratios of P_{CH4}/P_{H2}; (b) lateral growth rates as a function of hydrogen pressure; (c) Linear growth rates as function of $1/T$ for various P_{CH4}/P_{H2} ratios $\leq 1.81\times10^{-2}$.

The E_{det} and constant b can be extracted by analyzing the 'pure etching' regime without CH_4 presence (Figure S9). Since in this case, the first component of Equation 2 is zero, the slope of the linear fit of the etching rates in the Arrhenius coordinates gives $E_{det} = 2.0 \pm 0.1$ eV. Then by fitting the data points from the linear P_{CH4}/P_{H2} range (below 2×10^{-2}) in Figure 4c to Equation 2, we extract $E_{att} = 1.9 \pm 0.3$ eV. It is worth pointing out that in the present study we leave out the nucleation stage (which is not accessible) and probe exclusively the growth phase.

Previously for the CVD of graphene on solid copper, a growth energy barrier of 2.6 ± 0.5 eV was estimated by means of *ex situ* scanning electron microscopy (SEM).[22] The authors ruled out the process of CH_4 dissociative adsorption as the rate-limiting step of the graphene growth in favor of the carbon species attachment to the step-edge. However, the theoretical activation energies of CH_4 dissociation on solid Cu may exceed 3 eV as proposed by recent computational work.[39] A comparable value of the apparent E_a (2.3–2.5 eV) was measured by differential reflectance spectroscopy on the base of two wavelength 405 and 950 nm *in situ* on solid Cu in Ref.[25]. These experimental results are based on the areal growth rate on a solid substrate. On solid Ru and Ir, the attachment of C-clusters with an E_{att} of 2.0 eV instead of adatoms was proposed.[24,29] One study reports the growth E_a on liquid Cu extracted from the lateral size growth rates as 1.07 eV (in the presence of graphene/Mo_2C heterostructures).[40] The detachment energy was not taken into account in the above-mentioned studies. Alternatively, the E_a was found to be time-dependent due to the dispersive reaction kinetics of the ethylene precursor which affects the reaction through the rate of dissociative dehydrogenation with a high energy barrier of 3.1 eV.[23]

Free-energy surface simulations. To evaluate the hypothesis of a reaction-limited growth with the attachment process as the rate-limiting step, we conduct free-energy calculations by means of an MTP trained to DFT data. Here, we directly simulate the attachment process of a monomer or dimer carbon species to a zigzag graphene edge. These reaction steps are chosen as exemplary attachment processes whereby the attachment to the straight edge is most likely the least favorable (and most limiting) due to the creation of many dangling bonds. Further, we chose to simulate fully dehydrogenated carbon intermediates and graphene edges, which have also previously been proposed as the most stable[39] and that are the least error-prone in a computational treatment due to a reduced configurational space. To rationalize the interchangeability among different carbon intermediates we additionally model the dissociation of a carbon dimer to two monomers.

The free energy profiles of attachment/detachment of a carbon monomer and dimer to a graphene zigzag edge simulated by OPES are shown in Figure 5a,b. Considering the complete process, both net attachment and detachment barriers are highly similar with 1.66 ± 0.13 eV and 2.12 ± 0.01 eV

for the monomer and 1.71 ± 0.15 eV and 2.09 ± 0.02 eV for the dimer, respectively. The uncertainty for the attachment barriers is larger since the free energy of the detached state is difficult to converge due to the fast diffusion of free molecules (see Figure S16 in the SI). The high values obtained are in contradiction with a somewhat low theoretical attachment energy E_{att} of C dimers of 0.58 – 0.74 eV calculated with first-principal calculations for solid Cu.[41] The calculated attachment and detachment barriers are in very good agreement with the experimentally determined apparent activation energies for the growth and etching process, respectively. Our computational results, therefore, strongly support the proposed reaction-limited growth process found experimentally.

We also find an interesting behavior considering the attachment process of a dimer molecule to the graphene zigzag edge (Figure 5b). The attachment of both dimer carbon atoms to the edge is most favorable, which would suggest the predominant formation of a five-membered ring. Such a growth mechanism would eventually lead to a highly defective graphene sheet, which contradicts the common impression of high-quality graphene growth on liquid Cu. In fact, we find the detachment of one of the dimer atoms to be very facile with a barrier of 1.0 eV. This energy barrier, which is much lower than attachment barriers, suggests a dynamic opening of such five-membered rings which would result in a favorable self-alignment during growth and thereby to a defect-free graphene sheet. This observation is in line with the previously suggested defect-healing mechanism.[42]

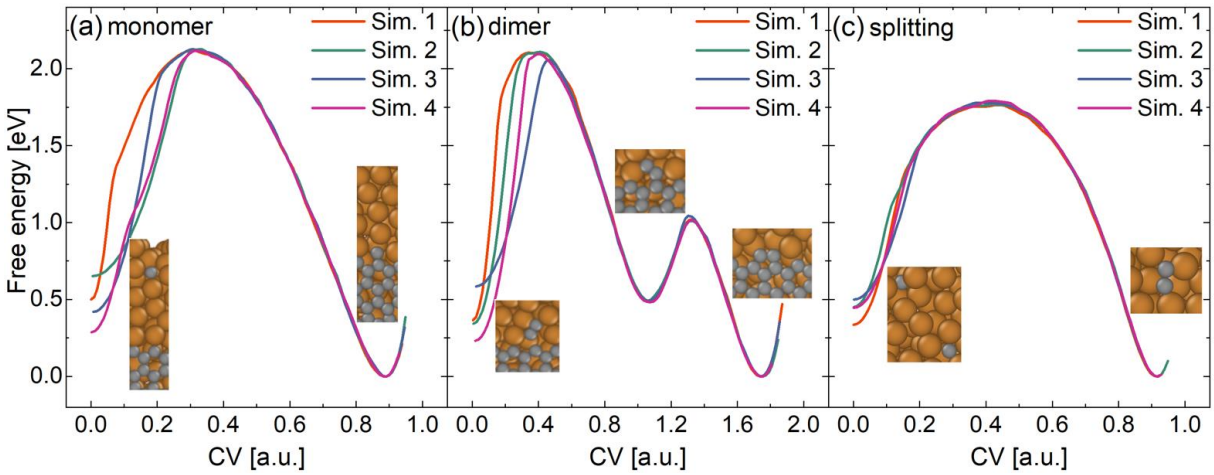

Figure 5. Free energy profiles of (a) the attachment/detachment of a carbon monomer and (b) a dimer to/from graphene zigzag edges; (c) the decomposition and formation of a carbon dimer to/from two monomers.

As shown in Figure 5c, the carbon dimer state is more favorable than the carbon monomer state, where a free energy difference in the bonding of ~0.5 eV is found. This energy difference possibly suggests a considerably larger share of dimer species than monomer species. The species

interconversion is also in the same order of magnitude as the growth process indicating that monomers and dimers cannot dynamically interconvert during growth. This is in line with the previous works suggesting that in the process of CH_4 chemisorption on solid Cu, the formation of carbon dimers C_2 is favored as the first nucleation step for the graphene domain growth.[16,43–45]

CONCLUSIONS

We investigated the CVD growth of graphene domains on a liquid copper catalyst by using real-time *in situ* optical microscopy in combination with free energy calculations. We found the flake morphology (varying between hexagonal and circular shapes) to be dependent strongly on the methane pressure as well as on the flake size, and almost independent of the temperature (in the T = 1368 – 1456 K range). Despite this fact, at constant pressures and temperature, the lateral growth rates reveal no time or size (from tens of μm up to 2 mm) dependence, staying constant within the wide experimental range. Hence, we propose the attachment of carbon active species to be the rate-limiting step with an activation energy of 1.9 ± 0.3 eV. The competing process of the detachment (etching) with a barrier of 2.0 ± 0.1 eV also has to be considered when analyzing the growth kinetics.

Our computational work shows that the attachment and detachment barriers of carbon intermediates quantitatively rationalize the experimentally observed apparent activation barriers. By comparing the carbon monomer with the carbon dimer, we find that the active carbon species is most likely the dimer. We also recover the previously suggested self-healing mechanism in our simulations.[42] Extended work treating more elementary growth steps and including hydrocarbon species will be the subject of future work.

These results contribute to the detailed understanding of the so far poorly investigated process of CVD growth of graphene on a liquid copper surface, thus being of high interest to the field of 2D materials synthesis technologies.

METHODS

Experimental details. We used a customized CVD reactor capable of multi-technique *in situ* monitoring to investigate the graphene growth on a liquid copper catalyst under CVD conditions.[46] As substrate, we used copper foils of high purity (99.9976%) purchased from Advent Research Materials (Eynsham, The United Kingdom) and tungsten disks from Metel BV (Waalwijk, The Netherlands) to support the molten copper. Before the first growth, we conditioned the copper foils by melting and etching them in a mixture of gaseous H_2 (9%) and Ar (91%) at a temperature $T \approx$ 1370 K for a few hours to remove oxides and bulk impurities. Argon and hydrogen were constantly

flown during operation with flows of 200 and 20 sccm, respectively. The total pressure in the reactor was kept at 200 mbar. We then proceeded to the graphene growth using a 2% gas mixture of methane in argon as a gas precursor. We varied its flow between 0 and 15 sccm, corresponding to partial pressure ratios P_{CH4}/P_{H2} between 0 and 2.72×10^{-2}. The graphene was grown on molten copper at the following temperatures T: 1368, 1399, 1416, 1433, and 1456 K with an uncertainty of 5 K. At the higher CH_4 flows, the growth occurs too rapidly to be thoroughly analyzed. But nevertheless, we extended the experimental range of P_{CH4}/P_{H2} by use of a 5% methane concentration in Ar in order to probe the range with the prevailing methane pressure based on the time required to cover the surface.

We monitored the CVD growth of graphene flakes on the liquid copper surface in real-time with a digital optical microscope used in radiation mode, mounted above a quartz window of the reactor.[12] We recorded the microscopic images using a CMOS-based digital camera (frame rate of 0.5 Hz) and analyzed them using scripts written in MATLAB software.

Computational details. The molecular simulations were conducted *via* a moment tensor potential (MTP)[47,48] for the Cu-C system, which is trained to the density functional theory (DFT) data computed with the Perdew-Burke-Ernzerhof (PBE) exchange-correlation functional[49] and the many-body-dispersion correction (PBE+MBD)[50]. This combination of machine learning potential and DFT has been demonstrated to be both accurate and efficient in our previous work.[51] To describe more complicated configurations encountered in the studied chemical reactions, we extended our previous potential by an active learning framework based on the ensemble method for uncertainty estimation as described in detail in the SI.[52]

Using the trained potential combined with the On-the-Fly-Probability-Enhanced-Sampling (OPES) approach,[53] we simulated free energy surfaces of three crucial processes during graphene growth at the liquid copper surface: the decomposition and formation of one carbon dimer from/to two monomers (mono-dimer), and the attachment of a carbon monomer or a dimer to graphene zigzag edges as supposedly the predominant edges for large scale graphene flake[54] (mono-ZZ and dimer-ZZ). Three relative atomic models, mono-dimer, mono-ZZ, and dimer-ZZ, are composed of C_2Cu_{260}, $C_{65}Cu_{877}$, and $C_{66}Cu_{877}$, respectively (compare SI Figure S13). For OPES calculations, collective variables (CV) should be defined to characterize the reaction process. Here we make use of the switching function:

$$s(r) = \frac{1-\left(\frac{r-d_0}{r_0}\right)^n}{1-\left(\frac{r-d_0}{r_0}\right)^m}, \quad (3)$$

in which r is the distance and d_0, r_0, n, m are parameters. We choose $d_0 = 0, r_0 = 2$ Å$, n = 6, m = 12$, and the functions transform the distance into a CV value in (0,1), as shown in Figure S14. For

the decomposition of the carbon dimers, r is the interatomic distance between two carbon atoms and $s(r)$ is the CV. This definition allows us to distinguish bonded and unbonded states: $s = 0$ means two monomers (no bond) while $s = 1$ means one dimer (bonded). $s(r)$ is also the CV for the attachment of the carbon monomers, but here r is the minimum distance between the monomer and the graphene layer, so $s = 0$ means the detached state while $s = 1$ means the attached state. And for the attachment of a carbon dimer, the CV is set as $s(r_1) + s(r_2)$, where r_1, r_2 are the minimum distances between the graphene and the two atoms of the dimer, respectively. Thus, the CV values of 0, 1, and 2 represent 3 states: the detachment state, the state in which only one atom is attached, and the state in which both atoms are attached. For each free energy surface, four independent OPES simulations of 4 ns with the same computational settings but different initial velocities are performed to evaluate mean values and uncertainties of the free energy barriers.

ACKNOWLEDGMENT

The authors thank European Union's Horizon 2020 research and innovation program under Grant Agreement No. 951943 (DirectSepa) for funding.

REFERENCES

(1) Yang, G.; Li, L.; Lee, W. B.; Ng, M. C. Structure of Graphene and Its Disorders: A Review. *Sci. Technol. Adv. Mater.* **2018**, *19* (1), 613–648.

(2) Tiwari, S. K.; Sahoo, S.; Wang, N.; Huczko, A. Graphene Research and Their Outputs: Status and Prospect. *J. Sci. Adv. Mater. Devices* **2020**, *5* (1), 10–29.

(3) K. S. Novoselov, A. K. Geim, S. V. Morozov, D. Jiang, Y. Zhang, S. V. Dubonos, I. V. G. and A. A. F. Electric Field Effect in Atomically Thin Carbon Films. **2004**, *306* (5696), 666–669.

(4) Yu, X.; Cheng, H.; Zhang, M.; Zhao, Y.; Qu, L.; Shi, G. Graphene-Based Smart Materials. *Nat. Rev. Mater.* **2017**, *2* (August), 1–14.

(5) Tiwari, S. K.; Mishra, R. K.; Ha, S. K.; Huczko, A. *Evolution of Graphene Oxide and Graphene: From Imagination to Industrialization*; 2018; Vol. 4.

(6) Kauling, A. P.; Seefeldt, A. T.; Pisoni, D. P.; Pradeep, R. C.; Bentini, R.; Oliveira, R. V. B.; Novoselov, K. S.; Castro Neto, A. H. The Worldwide Graphene Flake Production. *Adv. Mater.* **2018**, *30* (44), 1–6.

(7) Lin, L.; Peng, H.; Liu, Z. Synthesis Challenges for Graphene Industry. *Nat. Mater.* **2019**, *18* (6), 520–524.

(8) Jia, K.; Zhang, J.; Zhu, Y.; Sun, L.; Lin, L.; Liu, Z. Toward the Commercialization of Chemical Vapor Deposition Graphene Films. *Appl. Phys. Rev.* **2021**, *8* (4), 041306.

(9) Zheng, S.; Zeng, M.; Cao, H.; Zhang, T.; Gao, X.; Xiao, Y.; Fu, L. Insight into the Rapid Growth of Graphene Single Crystals on Liquid Metal via Chemical Vapor Deposition. *Sci. China Mater.* **2019**, *62* (8), 1087–1095.

(10) Liu, J.; Fu, L. Controllable Growth of Graphene on Liquid Surfaces. *Adv. Mater.* **2019**, *31* (9), 1–19.

(11) Tsakonas, C.; Dimitropoulos, M.; Manikas, A. C.; Galiotis, C. Growth and in Situ Characterization of 2D Materials by Chemical Vapour Deposition on Liquid Metal Catalysts: A Review. *Nanoscale* **2021**, *13* (6), 3346–3373.

(12) Jankowski, M.; Saedi, M.; La Porta, F.; Manikas, A. C.; Tsakonas, C.; Cingolani, J. S.; Andersen, M.; De Voogd, M.; Van Baarle, G. J. C.; Reuter, K.; et al. Real-Time Multiscale Monitoring and Tailoring of Graphene Growth on Liquid Copper. *ACS Nano* **2021**, *15*, 9638–9648.

(13) Tetlow, H.; Posthuma de Boer, J.; Ford, I. J.; Vvedensky, D. D.; Coraux, J.; Kantorovich, L. Growth of Epitaxial Graphene: Theory and Experiment. *Phys. Rep.* **2014**, *542* (3), 195–295.

(14) Li, X.; Cai, W.; Colombo, L.; Ruoff, R. S. Evolution of Graphene Growth on Ni and Cu by Carbon Isotope Labeling. *Nano Lett.* **2009**, *9* (12), 4268–4272.

(15) Li, X.; Cai, W.; An, J.; Kim, S.; Nah, J.; Yang, D.; Piner, R.; Velamakanni, A.; Jung, I.; Tutuc, E.; et al. Large-Area Synthesis of High-Quality and Uniform Graphene Films on Copper Foils. *Science* **2009**, *324* (5932), 1312–1314.

(16) Chen, H.; Zhu, W.; Zhang, Z. Contrasting Behavior of Carbon Nucleation in the Initial Stages of Graphene Epitaxial Growth on Stepped Metal Surfaces. *Phys. Rev. Lett.* **2010**, *104* (18), 1–4.

(17) Yazyev, O. V.; Pasquarello, A. Effect of Metal Elements in Catalytic Growth of Carbon Nanotubes. *Phys. Rev. Lett.* **2008**, *100* (15), 1–4.

(18) Song, J.; Kam, F. Y.; Png, R. Q.; Seah, W. L.; Zhuo, J. M.; Lim, G. K.; Ho, P. K. H.; Chua, L. L. A General Method for Transferring Graphene onto Soft Surfaces. *Nat. Nanotechnol.* **2013**, *8* (5), 356–362.

(19) Au, C.; Ng, C.; Liao, M. Methane Dissociation and Syngas Formation on Ru, Os, Rh, Ir, Pd, Pt, Cu, Ag, and Au: A Theoretical Study. *J. Catal.* **1999**, *185*, 12–22.

(20) Gan, L.; Luo, Z. Turning off Hydrogen to Realize Seeded Growth of Subcentimeter Single-Crystal Graphene Grains on Copper. *ACS Nano* **2013**, *7* (10), 9480–9488.

(21) Schwoebel, R. L.; Shipsey, E. J. Step Motion on Crystal Surfaces. *J. Appl. Phys.* **1966**, *37* (10), 3682–3686.

(22) Kim, H.; Mattevi, C.; Calvo, M. R.; Oberg, J. C.; Artiglia, L.; Agnoli, S.; Hirjibehedin, C. F.; Chhowalla, M.; Saiz, E. Activation Energy Paths for Graphene Nucleation and Growth on Cu. *ACS Nano* **2012**, *6* (4), 3614–3623.

(23) Celebi, K.; Cole, M. T.; Choi, J. W.; Wyczisk, F.; Legagneux, P.; Rupesinghe, N.; Robertson, J.; Teo, K. B. K.; Park, H. G. Evolutionary Kinetics of Graphene Formation on Copper. *Nano Lett.* **2013**, *13* (3), 967–974.

(24) Loginova, E.; Bartelt, N. C.; Feibelmarr, P. J.; McCarty, K. F. Factors Influencing Graphene Growth on Metal Surfaces. *New J. Phys.* **2009**, *11*.

(25) Tsakonas, C.; Manikas, A. C.; Andersen, M.; Dimitropoulos, M.; Reuter, K.; Galiotis, C. In Situ Kinetic Studies of CVD Graphene Growth by Reflection Spectroscopy. *Chem. Eng. J.* **2021**, *421* (P1), 129434.

(26) Geng, D.; Wu, B.; Guo, Y.; Huang, L.; Xue, Y.; Chen, J.; Yu, G.; Jiang, L.; Hu, W.; Liu, Y. Uniform Hexagonal Graphene Flakes and Films Grown on Liquid Copper Surface. *Proc. Natl. Acad. Sci. U. S. A.* **2012**, *109* (21), 7992–7996.

(27) Wu, B.; Geng, D.; Xu, Z.; Guo, Y.; Huang, L.; Xue, Y.; Chen, J.; Yu, G.; Liu, Y. Self-Organized Graphene Crystal Patterns. *NPG Asia Mater.* **2013**, *5* (1), e36-7.

(28) Tomellini, M.; Fanfoni, M. Mean Field Approach for Describing Thinfilm Morphology. *J. Phys. Condens. Matter* **2006**, *18* (17), 4219–4230.

(29) Loginova, E.; Bartelt, N. C.; Feibelman, P. J.; McCarty, K. F. Evidence for Graphene Growth by C Cluster Attachment. *New J. Phys.* **2008**, *10*.

(30) Ma, T.; Ren, W.; Zhang, X.; Liu, Z.; Gao, Y.; Yin, L. C.; Ma, X. L.; Ding, F.; Cheng, H. M. Edge-Controlled Growth and Kinetics of Single-Crystal Graphene Domains by Chemical Vapor Deposition. *Proc. Natl. Acad. Sci. U. S. A.* **2013**, *110* (51), 20386–20391.

(31) Seki, K. Scaling Theory for Two-Dimensional Single Domain Growth Driven by Attachment of Diffusing Adsorbates. *New J. Phys.* **2019**, *21* (9).

(32) Seki, K. On the Definition of the Domain Growth-Rate Constant on a Two-Dimensional Substrate. *J. Cryst. Growth* **2021**, *570* (June), 126222.

(33) Chernov, A. A. Notes on Interface Growth Kinetics 50 Years after Burton, Cabrera and Frank. *J. Cryst. Growth* **2004**, *264* (4), 499–518.

(34) Vlassiouk, I.; Regmi, M.; Fulvio, P.; Dai, S.; Datskos, P.; Eres, G.; Smirnov, S. Role of Hydrogen in Chemical Vapor Deposition Growth of Large Single-Crystal Graphene. *ACS Nano* **2011**, *5* (7), 6069–6076.

(35) Losurdo, M.; Giangregorio, M. M.; Capezzuto, P.; Bruno, G. Graphene CVD Growth on Copper and Nickel: Role of Hydrogen in Kinetics and Structure. *Phys. Chem. Chem. Phys.* **2011**, *13* (46), 20836–20843.

(36) Zhang, Y.; Zhang, L.; Kim, P.; Ge, M.; Li, Z.; Zhou, C. Vapor Trapping Growth of Single-Crystalline Graphene Flowers: Synthesis, Morphology, and Electronic Properties. *Nano Lett.* **2012**, *12* (6), 2810–2816.

(37) Meca, E.; Lowengrub, J.; Kim, H.; Mattevi, C.; Shenoy, V. B. Epitaxial Graphene Growth and Shape Dynamics on Copper: Phase-Field Modeling and Experiments. *Nano Lett.* **2013**, *13* (11), 5692–5697.

(38) Dong, J.; Zhang, L.; Ding, F. Kinetics of Graphene and 2D Materials Growth. *Adv. Mater.* **2019**, *31* (9), 1–29.

(39) Andersen, M.; Cingolani, J. S.; Reuter, K. Ab Initio Thermodynamics of Hydrocarbons Relevant to Graphene Growth at Solid and Liquid Cu Surfaces. *J. Phys. Chem. C* **2019**, *123*, 22299–22310.

(40) Turker, F.; Caylan, O. R.; Buke, G. Nucleation and Growth of Graphene/Mo2C Heterostructures on Cu through CVD. *J. Am. Ceram. Soc.* **2022**, *105* (2), 815–822.

(41) Wu, P.; Zhang, Y.; Cui, P.; Li, Z.; Yang, J.; Zhang, Z. Carbon Dimers as the Dominant Feeding Species in Epitaxial Growth and Morphological Phase Transition of Graphene on Different Cu Substrates. *Phys. Rev. Lett.* **2015**, *114* (21), 1–5.

(42) Li, H. B.; Page, A. J.; Hettich, C.; Aradi, B.; Köhler, C.; Frauenheim, T.; Irle, S.; Morokuma, K. Graphene Nucleation on a Surface-Molten Copper Catalyst: Quantum Chemical Molecular Dynamics Simulations. *Chem. Sci.* **2014**, *5* (9), 3493–3500.

(43) Gajewski, G.; Pao, C. W. Ab Initio Calculations of the Reaction Pathways for Methane Decomposition over the Cu (111) Surface. *J. Chem. Phys.* **2011**, *135* (6).

(44) Zhang, W.; Wu, P.; Li, Z.; Yang, J. First-Principles Thermodynamics of Graphene Growth on Cu Surfaces. *J. Phys. Chem. C* **2011**, *115* (36), 17782–17787.

(45) Chen, S.; Gao, J.; Srinivasan, B. M.; Zhang, G.; Sorkin, V.; Hariharaputran, R.; Zhang, Y. W. An All-Atom Kinetic Monte Carlo Model for Chemical Vapor Deposition Growth of Graphene on Cu(1 1 1) Substrate. *J. Phys. Condens. Matter* **2020**, *32* (15).

(46) Saedi, M.; De Voogd, J. M.; Sjardin, A.; Manikas, A.; Galiotis, C.; Jankowski, M.; Renaud, G.; La Porta, F.; Konovalov, O.; Van Baarle, G. J. C.; et al. Development of a Reactor for the in Situ Monitoring of 2D Materials Growth on Liquid Metal Catalysts, Using Synchrotron X-Ray Scattering, Raman Spectroscopy, and Optical Microscopy. *Rev. Sci. Instrum.* **2020**, *91*, 013907.

(47) Shapeev, A. V. Moment Tensor Potentials: A Class of Systematically Improvable Interatomic Potentials. *Multiscale Model. Simul.* **2016**, *14* (3), 1153–1173.

(48) Novikov, I. S.; Gubaev, K.; Podryabinkin, E. V; Shapeev, A. V. The MLIP Package: Moment Tensor Potentials with MPI and Active Learning. *Mach. Learn. Sci. Technol.* **2021**, *2* (2), 025002.

(49) Perdew, J. P.; Burke, K.; Ernzerhof, M. Generalized Gradient Approximation Made Simple. *Phys. Rev. Lett.* **1996**, *77* (18), 3865–3868.

(50) Hermann, J.; Tkatchenko, A. Density Functional Model for van Der Waals Interactions: Unifying Many-Body Atomic Approaches with Nonlocal Functionals. *Phys. Rev. Lett.* **2020**, *124* (14), 146401.

(51) Gao, H.; Belova, V.; Porta, F. La; Cingolani, J. S.; Andersen, M.; Saedi, M.; Konovalov, O. V; Jankowski, M.; Heenen, H. H.; Groot, I. M. N.; et al. Graphene at Liquid Copper Catalysts : Atomic-Scale Agreement of Experimental and First-Principles Adsorption Height. *Adv. Sci.* **2022**, 2204684.

(52) Musil, F.; Willatt, M. J.; Langovoy, M. A.; Ceriotti, M. Fast and Accurate Uncertainty Estimation in Chemical Machine Learning. *J. Chem. Theory Comput.* **2019**, *15* (2), 906–915.

(53) Invernizzi, M.; Parrinello, M. Rethinking Metadynamics: From Bias Potentials to Probability Distributions. *J. Phys. Chem. Lett.* **2020**, *11* (7), 2731–2736.

(54) Shu, H.; Chen, X.; Ding, F. The Edge Termination Controlled Kinetics in Graphene Chemical Vapor Deposition Growth. *Chem. Sci.* **2014**, *5* (12), 4639–4645.